Journal of Power Sources 195 (2010) 3374–3379

Contents lists available at ScienceDirect

Journal of Power Sources

journal homepage: www.elsevier.com/locate/jpowsour

Low Pt content on the $Pd_{45}Pt_5Sn_{50}$ cathode catalyst for PEM fuel cells

J.J. Salvador-Pascual[a], V. Collins-Martínez[b], A. López-Ortíz[b], O. Solorza-Feria[a,*]

[a] Depto. Química, Centro de Investigación y de Estudios Avanzados del IPN, A. Postal 14-740, 07360 México D.F., Mexico
[b] Centro de Investigación en Materiales Avanzados, Miguel de Cervantes 120, 31109 Chihuahua, Mexico

ARTICLE INFO

Article history:
Received 25 October 2009
Received in revised form
11 December 2009
Accepted 11 December 2009
Available online 21 December 2009

Keywords:
Oxygen reduction reaction
$Pd_{45}Pt_5Sn_{50}$ electrocatalyst
Electrocatalyst synthesis
PEMFC performance

ABSTRACT

$Pd_{45}Pt_5Sn_{50}$ electrocatalyst was prepared by a $NaBH_4$ reduction of $PdCl_2$, H_2PtCl_6 and $SnCl_2$ in THF at 0 °C. This catalyst was characterized by X-ray diffraction (XRD), transmission electron microscopy (TEM), scanning electron microscopy (SEM), energy dispersive X-ray spectrometry (EDS) microanalysis and hydrodynamic electrochemical technique. XRD, SEM and TEM results demonstrate that the borohydrate reduction methodology enable the synthesis of conglomerated particles nanometric in size ranging from 1 to 6 nm. Oxygen reduction reaction (ORR) activity was investigated on carbon dispersed catalyst by rotating disk electrode (RDE) technique in H_2SO_4 0.5 M. The effect of temperature on the kinetics was analyzing resulting in an apparent activation energy of 42.54 ± 1 kJ mol^{-1}, value which is less than the obtained for the nanostructured bimetallic PdSn electrocatalyst under the same experimental condition. The $Pd_{45}Pt_5Sn_{50}$ electrocatalyst dispersed on a carbon powder was tested as cathode electrocatalyst in a membrane-electrode assembly (MEA) arriving to a power density of 210 mW cm^{-2} at 0.35 V and 80 °C.

1. Introduction

Fuel cells and metal-air batteries offer attractive alternative power source for stationary and portable applications in relation to traditional fossil-fuel energy production, conversion and storage. However, one critical issue to be addressed is the lack of effective electrocatalysts for multi-electron charge transfer processes of oxygen reduction at low overpotential. The cathodic overpotential is strongly influenced by several physical parameters such as electrocatalysts intrinsic properties, active catalysts surface area, concentration and diffusion coefficient of the oxygen and so on. The novel electrocatalysts are specially aimed to promote the dissociation of the O–O bond during the oxygen reduction reaction (ORR) mechanism, and to maintain reactivity and selectivity on the electrode surface [1–6]. Multi-metallic and alloy catalysts have been particularly active area of research because it has been established that for the cathode reaction, multi-metallic surfaces have superior activity to pure metal [7,8]. The enhanced reactivity of the catalysts surfaces is attributed to their electronic and geometric structure associated to the bi-functional effects, in which the unique catalytic properties of each of the elements in the catalytic compound combine in a synergetic manner to yield a surface which results more active than each of the elements alone. Also an electronic effect could modify the electronic properties of the alloy to enhance the active catalytic surface. Among the electrocatalysts that have shown interesting electrochemical properties both in terms of tolerance to alcohol and high activity toward the ORR are Pd- and Pd-alloys [9,10]. Recently, we have shown that Pd [11] and Pd-based catalysts [12,13], such as PdSn of nanometric sizes exhibited an attractive catalytic activity for the ORR, but limited by the stability of the catalyst in acid media. The interest of this work in developing palladium thin bimetallic compound bearing low concentration of platinum atoms is to improve the stability and avoid the lixiviation of the bimetallic compound as well as to reinforce the electrocatalytic activity for the ORR through the synergistic effects of the three metals. The effect of temperature on the kinetics of the ORR study of the $Pd_{45}Pt_5Sn_{50}$ catalyst and the performance response of this cathode catalyst in a membrane-electrode assembly also constitutes part of this work.

2. Experimental

2.1. Physical and chemical characterizations

At present, there are several methods for synthesizing supported and unsupported nanomaterials based on nanoparticles catalysts of various controllable sizes. $Pd_{45}Pt_5Sn_{50}$ electrocatalyst with low content of Pt was prepared by a $NaBH_4$ (0.06 M) reduction of $PdCl_2$ (0.86 mM), H_2PtCl_4 (0.086 mM) and $SnCl_2$ (0.86 mM) in a 100 mL tetrahydrofuran solution, THF a 0 °C, following the methodology we have reported previously for the preparation of nanometric Pd-based electrocatalysts [11–13]. Briefly, a chemical reactor was charged with the reagents and vigorously stirred for the chemicals solvation. Afterwards, $NaBH_4$ (0.06 mM) solution

* Corresponding author. Tel.: +52 55 5747 3715; fax: +52 55 5747 3389.
E-mail address: osolorza@cinvestav.mx (O. Solorza-Feria).

0378-7753/$ – see front matter © 2009 Elsevier B.V. All rights reserved.
doi:10.1016/j.jpowsour.2009.12.045

was slowly added maintaining the stirred solution at 0 °C under N_2 atmosphere for 16 h. The reaction product was washed with distilled water to eliminate the sodium chloride formed during the reaction. After filtered, the powder was dried and weighted obtaining a 99% of yield. The powder was subject to thermal treatment under H_2 atmosphere (4 bar) at 573 K for 3 h following a procedure described for Sn-bimetallic alloys [14,15], in order to avoid Sn lixiviation in the alloy as observed previously during the electrochemical activation process. The afterward the resulted powder was cooled down obtaining a yield of 91% and maintained in a closed recipient prior to optical and electrochemical characterization.

2.2. Physical characterization

Phase identification of the powdered catalyst, after thermal treatment, was carried out with a MPD Phillips diffractometer equipped with Cu Kα radiation and a graphite monocromator (λ = 0.1542 nm). Scanning steps of 0.02° 2θ were used in the range of 30–90° 2θ. Particle size was determined from transmission electron microscopy (TEM) analyses, using a CM200 Phillips microscope, operated at 200 keV and equipped with energy dispersive spectroscopy (EDS) used to obtain an average and local chemical composition of the samples. For superficial studies, a Leica-Cambridge Stereoscan 440 SEM, at 20 kV, was used to analyze the morphology and distribution of the elements in the materials.

2.3. Electrochemical characterization

For electrochemical studies, experiments were carried out in a temperature controlled double compartment three-electrode test cell. A platinum mesh was used as the counter electrode and $Hg/Hg_2SO_4/0.5\,M\ H_2SO_4$ (MSE = 0.680 V/NHE) as reference electrode. This electrode was outside the cell, kept at room temperature and connected by a porcelain Luggin capillary close to the surface of the working electrode. The electrode potentials were referred to NHE. The electrolyte was a 0.5 M H_2SO_4 solution prepared from double-distilled water which was degassed with N_2 for the working electrode activation and saturated with O_2 for 20 min before each ORR electrochemical measurements. Electrochemical studies were performed in a Voltalab potentiostat. Cell temperature was controlled by a Haake thermostat (model F3) from 308 to 333 K. Rotating disk electrode, RDE measurements were conducted on a thin film catalyst deposited on a glassy carbon disk electrode (0.196 cm^2) mounted in a interchangeable RDE holder (Pine Instruments). The glassy carbon ink-type working electrode disk was prepared according to a method reported previously [16,17]. The thin film was deposited from a solution which was prepared by adding 5 μL of a suspension resulting by mixing 45 μL 2-propanol, 5 μL Nafion® (5 wt.%, Du Pont 1000EW) and 1 mg $Pd_{45}Pt_5Sn_{50}$ (50 wt.%/C). The estimated amount of catalyst in the thin film was about 0.5 mg cm^{-2}. The rotation rate of the working electrode was in the range of 200 and 2500 rpm at 5 mV s^{-1}. During the ORR measurements an oxygen flux was maintained above the electrolyte surface.

2.4. Membrane-electrode assembly (MEA) preparation and characterization

The anodic catalysts layer was prepared by spraying a suspension of ink containing a mixture of a 20 wt.% Pt/C (E-Tek) electrocatalyst in one side of a Nafion 115 membrane. The catalytic ink was prepared by mixing 14 mL of Nafion 5 wt.% (Du Pont, 1100EW), 240 mL of isopropanol, 5 mg of the supported Pt/C and sonicated for 20 min. The resulting suspension was sprayed onto the 115 Nafion membrane by means of a home fabricated semiautomatic device. The anodic and cathodic loading in both catalyst layers was about 1.0 mg cm^{-2}. The cathode catalytic ink was prepared following the same procedure as described for the anode side by mixing 5 mg of $Pd_{45}Pt_5Sn_{50}$ with 7.5 mg of Vulcan carbon XC-72 and the resulted suspension sprayed onto the cathodic side of the 115 Nafion membrane. The gas diffusion medium at the anode and cathode side was Teflon-treated carbon paper (Electrochem). The MEA was obtained by hot pressing (4.4 kg cm^{-2}) at 120 °C for 1 min. The active surface area of the anode and cathode was 5 cm^2. PEMFC test was carried out in an Electrochem Fuel Cell Test System 890B operated with high purity hydrogen and oxygen at 400 cm^3 min^{-1}. The fuel cell performance was measured at 40 °C, 60 °C and 80 °C without pressure of both gases. The fuel cell station was equipped with a humidifying system for the reactant gases and the humidified temperatures were fixed 5 °C higher than the fuel cell temperature.

3. Results and discussions

3.1. Characterization of the prepared $Pd_{45}Pt_5Sn_{50}$ catalyst

X-ray diffraction results of PdSn and $Pd_{45}Pt_5Sn_{50}$ compounds synthesized under the same experimental conditions are shown in Fig. 1. Synthesized PdSn [13] showed an orthorhombic structure Pnma, which experimental XRD pattern matches well the standard JCPDS card 03-065-2603. Narrow peaks in the PdSn XRD pattern indicate the presence of nanocrystallites which percentage, about 90%, was determined by MDI jade 5.0 software. The average size of the PdSn catalyst, about 8.6 nm (Rpw 10.3), was deduced by fitting the diffraction patterns using the academic Topas software. Low Pt concentration addition changes the bulk structure of the palladium thin bimetallic compound as shown in XRD and TEM results: XRD pattern of $Pd_{45}Pt_5Sn_{50}$ showed a reduced number of peaks in relation to obtained on PdSn, fitting in almost all the cases with structural Pd face-centered cubic (fcc) package (JCPDS card 046-1043), Pt (JCPDS card 04-0802) and Sn (JCPDS card 04-0673). However, crystalline faces positioned at 2θ = 52°, 58° and 80° not correspond to the lattice phase of the three metals of the compound, revealing the alloy formation between Pd, Pt and Sn. These new phases are associated to strong interactions between the three metallic atoms which enhanced the stability of the $Pd_{45}Pt_5Sn_{50}$ compound in relation to that of Pd alone [11]. The average crystallite size of the PdSn catalyst, about 6.3 nm (Rpw 10.3), was

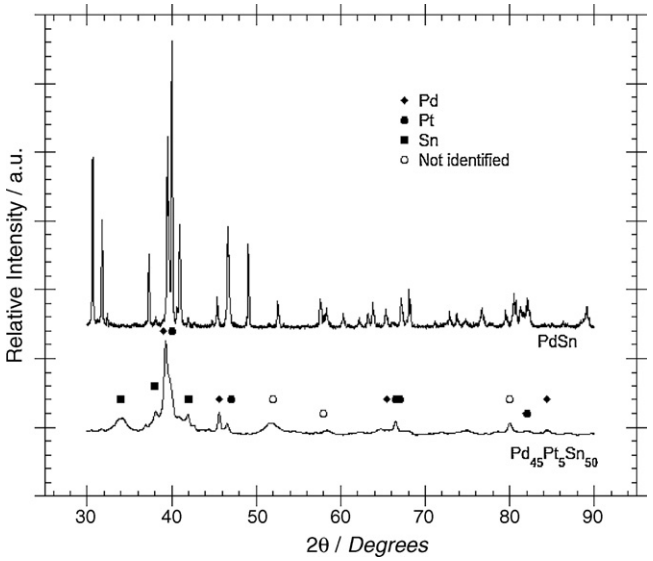

Fig. 1. XRD patterns of nanosized particles of PdSn and $Pd_{45}Pt_5Sn_{50}$ catalysts as-synthesized by the borohydride reduction method.

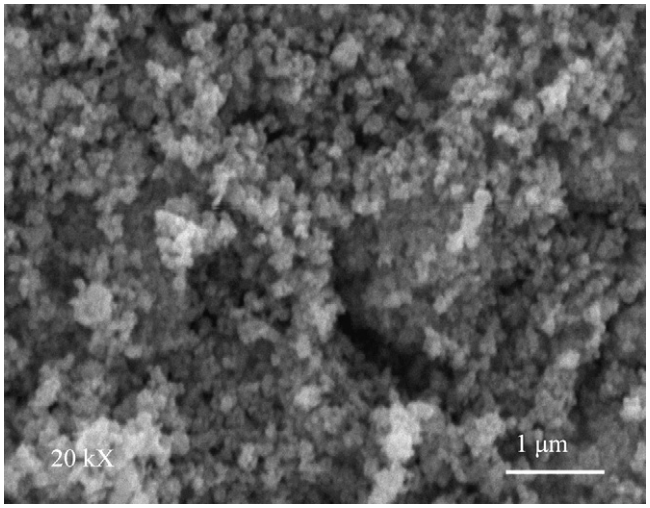

Fig. 2. SEM micrograph of $Pd_{45}Pt_5Sn_{50}$ catalyst synthesized by the $NaBH_4$ reduction method in THF at 0 °C.

deduced by fitting the diffraction patterns using the same academic Topas software mentioned above. Broad peaks in the $Pd_{45}Pt_5Sn_{50}$ diffraction peaks suggest low crystallinity which percentage about 30% was also determined by using the same software. Studies by SEM, Fig. 2, showed a homogenous distribution of spherical powder agglomerates composed of numerous powder particles having sizes less than 100 nm. Notice that these particle sizes are still much larger than the calculated crystallite size (~6 nm), indicating that the particles are nanocrystalline, a common feature reported for materials produced by the $NaBH_4$ reduction process [11]. The average composition of the as-synthesized powders, as determined by EDS, was approximately 45 at% Pd, 5 at% Pt and 50 at% Sn ($Pd_{45}Pt_5Sn_{50}$), in concordance with the started estimated composition of synthesis. The morphology of $Pd_{45}Pt_5Sn_{50}$ was analyzed by TEM and results exhibited spherical agglomerates which are built of fine particles. Fig. 3 shows a TEM micrograph of $Pd_{45}Pt_5Sn_{50}$ particle sizes catalyst of around 1–6 nm which are agglomerated in a greatest degree of clustering spherical particles in a range of 100 nm.

Fig. 4 shows mapping images for the $Pd_{45}Pt_5Sn_{50}$ sample where a uniform distribution of elemental palladium, platinum and tin throughout the particle with no evidence of metal segregation within the mapped area is observed.

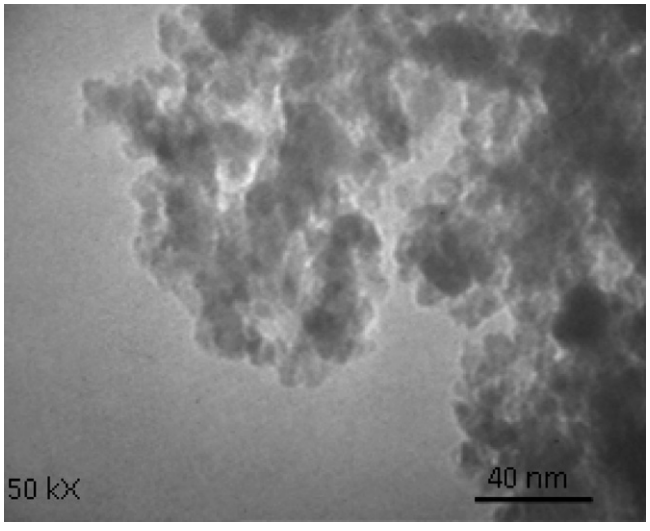

Fig. 3. TEM micrograph of $Pd_{45}Pt_5Sn_{50}$ catalyst synthesized by the borohydride reduction method.

These results of XRD, SEM-EDS and TEM indicate that the as-synthesized $Pd_{45}Pt_5Sn_{50}$ powder mixtures consist mostly of powder agglomerates in which palladium, platinum and thin particles are intimately mixed.

3.2. Electrochemical study of oxygen reduction

Fig. 5 presents the final cycle from a typical voltamperometric cyclic activation process for the PdSn and $Pd_{45}Pt_5Sn_{50}$ samples. These voltamperograms indicate the characteristic behavior of PdSn, showing that with the incorporation of Pt its electrochemical response is modified in the anodic and cathodic regions. Well-defined typical adsorption/desorption peaks are observed on the $Pd_{45}Pt_5Sn_{50}$ catalyst in the region of 0.0–0.35 V/NHE. In the region the 0.5–1.2 V/NHE the adsorption of H_2O at the electrode surface is notorious and shift of the onset potential for the cathodic reaction on the $Pd_{45}Pt_5Sn_{50}$ is detected. An increase in the obtained ORR current density can be observed, thus indicating that the $Pd_{45}Pt_5Sn_{50}$ catalyst possess a higher oxygen adsorption capacity than PdSn alone.

The oxygen reduction reaction is a complex combination of charge transfer and mass transport processes which by the low concentration of oxygen in acid environment, is usually studied under hydrodynamic conditions. Fig. 6 shows hydrodynamic behavior of the $Pd_{45}Pt_5Sn_{50}$ catalysts with Vulcan carbon powder dispersed into a Nafion film coated on a glassy carbon in oxygen saturated 0.5 M H_2SO_4 at 25 °C. The polarization curves were recorded from the open circuit potential to 0.2 V versus NHE. A charge transfer kinetics control with rotation rate-independent current is observed in the range of 0.75–0.90 V/NHE; at more cathodic potentials, mixed control became significant arriving to a well-defined mass transport-limited current as a function of the rotation rate. A different behavior was observed for Pd [11] and PdSn nanoparticles catalyst [13] where only mixed kinetic-diffusion control was clearly observed, regardless of the electrode rotation rates. It was considered that increases in the limiting current on high performance electrocatalysts are associated with the increase of molecular oxygen diffusion in the boundary-layer thickness through the electrode surface. The reduction reaction is fast enough at high cathodic overpotentials, associated in almost all the cases to a flat limiting plateau as described for a Pt/C electrode [18]. An explanation for the well-defined current plateau could be attributed to a distribution of electrocatalytic active sites on the electrode surface such as observed in the mapping of Fig. 4. In a film-coated electrode surface, the overall measured current, i, is related to the kinetic current, i_k, the boundary-layer diffusion-limited current, i_d, and film diffusion-limited current, i_f by [19]

$$\frac{1}{i} = \frac{1}{i_k} + \frac{1}{i_d} + \frac{1}{i_f} \quad (1)$$

i_f represents the film diffusion-limited current controlled by reactant diffusion in the i_f Nafion® layer and is given by the following equation:

$$i_f = \frac{n_e F D_f C_f}{\delta_f} \quad (2)$$

In this equation, D_f and C_f are the diffusion coefficient and the concentration of O_2 in the film, respectively, and δ_f is the film thickness. The effect of the film diffusion is significant only in the case when the electrode is covered by a Nafion film [19,20] and can be neglected in the present study since the amount of Nafion (5 μL 5 wt.% in 45 μL of solution) in the prepared catalyst suspension is sufficiently small and hence not expected to be a factor in the limiting current density on the rotating electrode where only 5 μL of

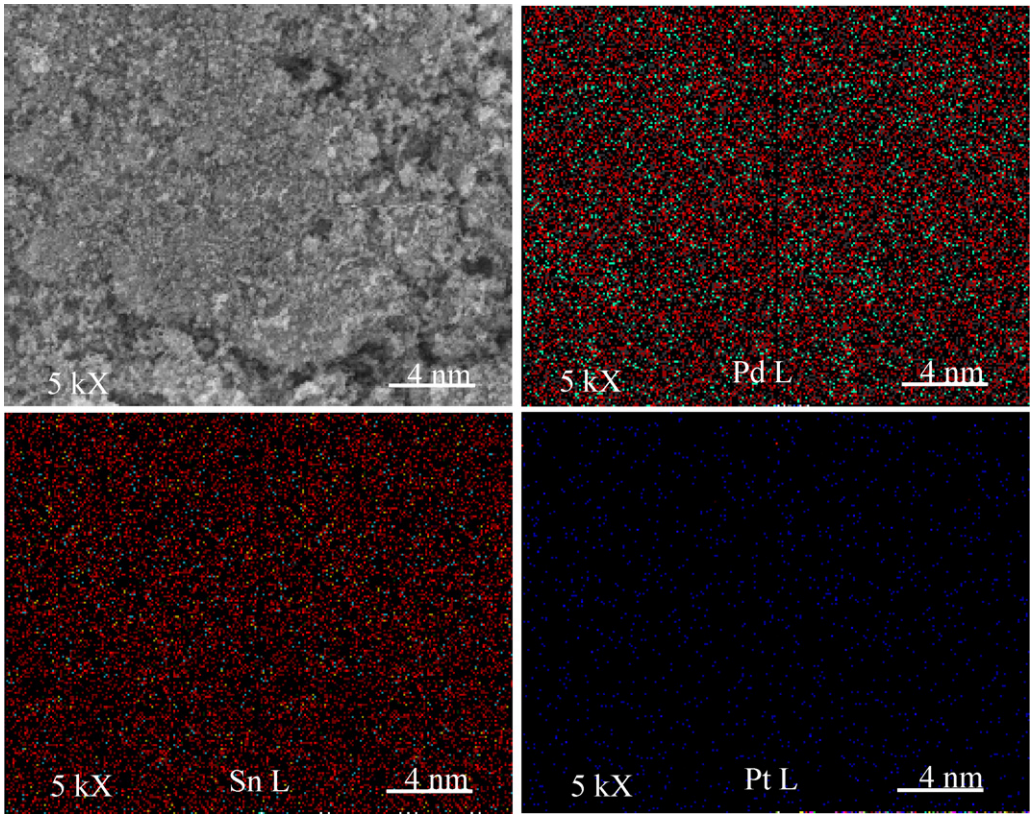

Fig. 4. Mapping images of the components of the $Pd_{45}Pt_5Sn_{50}$ catalyst.

catalyst ink is loaded. The boundary-layer diffusion-limited current can be expressed as

$$i_d = 0.2 n_e F C_o D_o^{2/3} \nu^{-1/6} \omega^{1/2} = B\omega^{1/2} \quad (3)$$

where 0.2 is a constant used when ω is expressed in revolution per minute, n_e is the number of electrons transferred per molecule of O_2 in the overall reaction, F the Faraday constant, C_o the concentration of oxygen dissolved (1.1×10^{-6} mol cm^{-3}), D_o the diffusion coefficient of oxygen in the solution (1.4×10^{-5} cm^2 s^{-1}), ν the kinematic viscosity of the sulfuric acid (1.0×10^{-2} cm^{-2} s^{-1}) [21] and B the Levich constant. The current of the oxygen reduction reaction can be written as dependent on the kinetic current and the diffusion-limited current as shown in the following equation:

$$\frac{1}{i} = \frac{1}{i_k} + \frac{1}{i_d} = \frac{1}{i_k} + \frac{1}{B\omega^{1/2}} \quad (4)$$

From the data of Fig. 6, the Koutecky–Levich plots (i^{-1} vs. $\omega^{-1/2}$) were drawn (figure not included). At all the rotation speeds, a series of essentially parallel straight lines in a broad potential range was observed, which indicates that the reaction order for the O_2 reduction at a $Pd_{45}Pt_5Sn_{50}$ catalyst electrode is unity, similar to observed and reported previously on PdSn [13]. Fig. 7 shows the mass transport corrected Tafel plots obtained for the $Pd_{45}Pt_5Sn_{50}$ catalyst ink-type electrode on which oxygen reduction kinetics studies were conducted in 0.5 M H_2SO_4 at 298 K. Electrochemical polarization curves on Pd, PdSn and Pt were also included in this figure for comparison. The Tafel plots were obtained after the measured currents were corrected for diffusion to give the kinetic currents in the mixed activation-diffusion region, calculated from Eq. (4):

$$i_k = \frac{i i_d}{i_d - i} \quad (5)$$

where $i_d/(i_d - i)$ is the mass transfer correction. The Tafel plots show a linear behavior in the mixed activation-diffusion region and a deviation of the kinetic current occurs with higher slope at high current density. A Tafel slope of -40 mV dec^{-1}, charge transfer coefficient of 0.68 and an exchange current density of 3.35×10^{-4} mA cm^{-2} was determined on $Pd_{45}Pt_5Sn_{50}$ at 308 K. The kinetic parameters deduced for the oxygen reduction on all the catalysts ink-type electrodes at 308 K are presented in Table 1.

The effect of temperature on the kinetic parameters of the $Pd_{45}Pt_5Sn_{50}$ electrocatalyst is of paramount importance in the cathodic reaction of a fuel cell. The oxygen reduction was per-

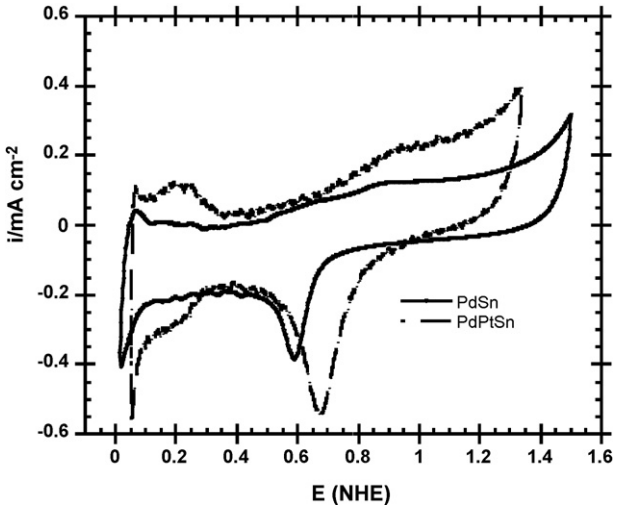

Fig. 5. Cyclic voltammetry of PdSn and $Pd_{45}Pt_5Sn_{50}$ catalysts in oxygen free 0.5 M H_2SO_4 solution at 298 K. Scan rate potential of 50 mV s^{-1}.

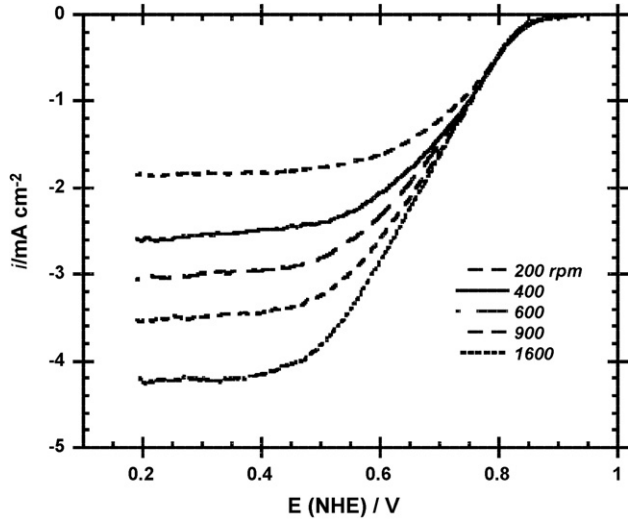

Fig. 6. Current–potential curves of ORR at $Pd_{45}Pt_5Sn_{50}$ catalyst in 0.5 M H_2SO_4 saturated with O_2 at 308 K, at different rotation rates. Current recorded at 5 mV s^{-1}.

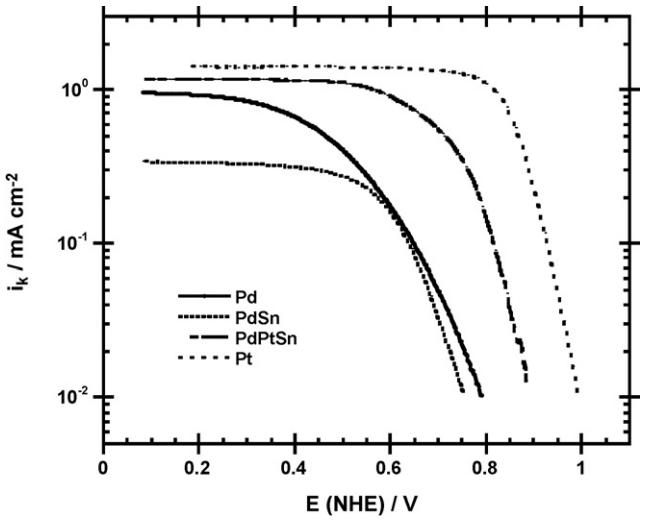

Fig. 7. Mass transfer corrected Tafel plots for ORR in O_2 saturated 0.5 M H_2SO_4 at 308 K of different Pd-based ink-type electrocatalysts deposited on glassy carbon. Pt is depicted as comparison.

formed on a RDE by recording current–potential curves, similar to reported in Fig. 6, for each cell temperature. The mass transfer corrected current–potential curves at various temperatures are shown in Fig. 8. Effects such as the increase of the catalytic current and shift of the curves to more positive potentials were observed from increasing temperatures. As expected, the kinetics of the electrochemical reaction is higher at elevated temperatures, reflecting the temperature dependence of the chemical rate constant. This behavior is indicative of an enhancement of the electrocatalytic kinetic reduction of the adsorbed oxygen with temperature. To evaluate the exchange current density, i_o, and the charge transfer coefficient, α, from the Tafel slope as function of temperature, the dependence of the reversible oxygen electrode potential, E_r, on temperature

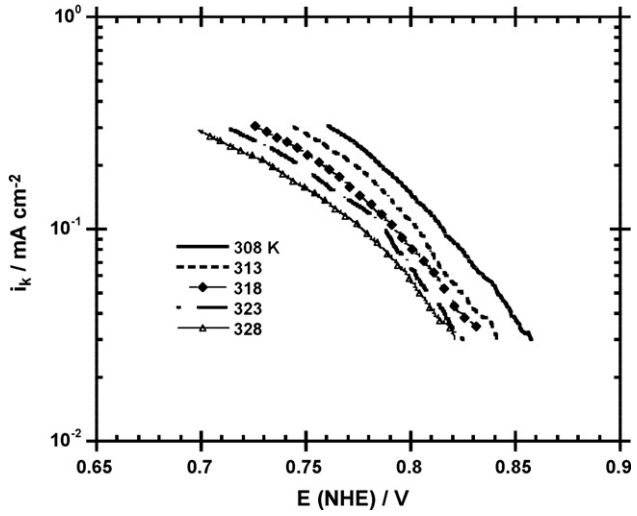

Fig. 8. Mass transfer corrected Tafel plots for the ORR on $Pd_{45}Pt_5Sn_{50}$ catalyst at different temperatures.

Table 2
Variation of kinetic parameters with temperature for ORR on $Pd_{45}Pt_5Sn_{50}$ electrocatalyst in 0.5 M H_2SO_4.

T (K)	α	$-b$ (mV dec^{-1})	i_0 (mA cm^{-2})
308	0.68	40.0	3.352×10^{-4}
313	0.62	43.0	4.390×10^{-4}
318	0.68	39.9	6.353×10^{-4}
323	0.68	40.7	5.720×10^{-4}
328	0.65	47.9	10.41×10^{-4}

[13] was evaluated using the value of ΔG° (H_2–O_2 cell) at each temperature using equations (6a) and (6b):

$$\Delta G^\circ_{(H_2/O_2)} = -296,658 - 33.6T \ln T + 389.8T, \quad (\mathrm{J\,mol^{-1}}) \qquad (6a)$$

$$E_r = \frac{-\Delta G^\circ_{(H_2/O_2)}}{2F} \qquad (6b)$$

Tafel slopes and kinetic parameters deduced from the linear part at each temperature of Fig. 8, are presented in Table 2. One can see that Tafel slope is practically invariant with temperature, leading to a dependence of the transfer coefficient with temperature. Table 2 shows Tafel slopes are invariant with temperature and are closely equal to −120 mV at all temperatures, *i.e.* to $2.3 \times 2RT/(\alpha F)$.

The exchange current density corresponding to each Tafel slope was calculated by extrapolating the potential to the E_r value at the experimental operating cell temperature. The temperature dependence of the exchange current density in Table 2 can be analyzed via conventional Arrhenius plot (Fig. 9). The apparent activation energy, $\Delta E^{\neq}$, for the oxygen reduction reaction on $Pd_{45}Pt_5Sn_{50}$ electrocatalyst was evaluated in the temperature range of 308–333 K, from a linear regression analysis of the slope of the Arrhenius equation represented by the relationship

$$\Delta E^{\neq} = -2.3R \left[\frac{d \log i_0}{d(1/T)}\right] \qquad (7)$$

Table 1
Kinetic parameters deduced from the oxygen reduction reaction in 0.5 M H_2SO_4 at 298 K.

Electrocatalysts	E_{oc} (NHE V^{-1})	$-b$ (V dec^{-1})	α	i_o (mA cm^{-2})	Potential/V at i = 0.1 mA cm^{-2}	Ref.
Pd	0.78	0.131	0.46	6.6×10^{-6}	0.647	[11]
PdSn	0.80	0.056	0.46	1.606×10^{-6}	0.64	[13]
$Pd_{45}Pt_5Sn_{50}$	0.90	0.068	0.40	3.352×10^{-4}	0.81	

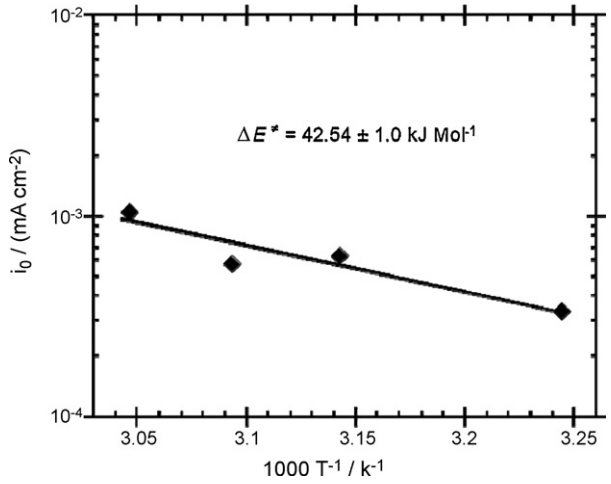

Fig. 9. Electrochemical Arrhenius plot deduced from the exchange current density of the corrected data of Fig. 8.

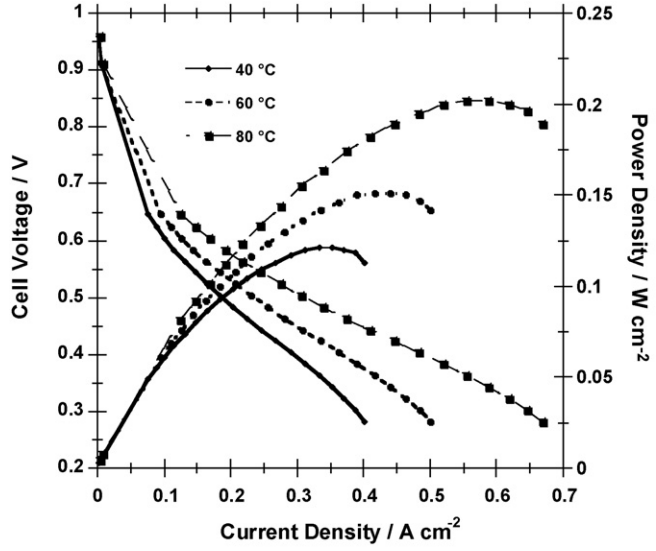

Fig. 10. Performance curve for Pt (20 wt.%/C) anode/$Pd_{45}Pt_5Sn_{50}$ (40 wt.%/C) cathode, operating on H_2/O_2 at 80 °C.

An average value of $\Delta E^{\neq} = 42.54 \pm 0.08\,kJ\,mol^{-1}$ was calculated. This value is lower in comparison to that of nanometric Pd (89.8 kJ mol^{-1}) [11] and PdSn (53.18 kJ mol^{-1}) [13] electrocatalysts. This result indicates that the incorporation of low concentration of platinum to a palladium tin bimetallic compound improves the catalytic activity and selectivity of the $Pd_{45}Pt_5Sn_{50}$ electrocatalyst towards the reduction of molecular oxygen in acid medium to water formation. The performance of the $Pd_{45}Pt_5Sn_{50}$ (20 wt.%) carbon supported catalyst produced by $NaBH_4$ reduction, synthesized and used as cathode electrode in polymer membrane fuel cell will be the subject of forthcoming communications.

3.3. PEMFC performance

Fig. 10 shows result of the MEA performance of the anode, Pt 20 wt.%/C (E-tek) with a catalyst loading of 1.0 mg cm^{-2}, and cathode catalyst loading (1.0 mg cm^{-2}) of $Pd_{45}Pt_5Sn_{50}$ 20 wt.% dispersed on Vulcan carbon, tested at 40 °C, 60 °C and 80 °C. An increase of the power density was observed with temperature. The maximum performance obtained under this experimental condition was 210 mW cm^{-2} at 0.35 V and 80 °C. The performance of $Pd_{45}Pt_5Sn_{50}$/Vulcan carbon was about 46% lower than MEA Pt performance reported by our group in Ref. [1]. This behavior is attributed to the low Pt content in the $Pd_{45}Pt_5Sn_{50}$ catalyst and by using the same catalyst loading on anodic and cathodic side, situation which could be improved by thorough loading study on the MEA cathodic side. Further study is carried out in our group of research in order to properly support the catalyst to improve the electrochemical behavior and to determine the long term stability of the $Pd_{45}Pt_5Sn_{50}$ as cathode in a PEMFC.

4. Conclusions

The borohydride reduction process has been proven to be a significant synthetic tool for the preparation of spherical powder agglomerates composed of $Pd_{45}Pt_5Sn_{50}$ catalyst, with particles less than 100 nm, containing crystallites of around than 6 nm in size. The electrocatalytic activity of this compound, for the oxygen reduction reaction in acid media, showed that the electrocatalyst allowed multi-electron charge transfer to water formation, with an apparent activation energy of $42.54 \pm 0.08\,kJ\,mol^{-1}$. The $Pd_{45}Pt_5Sn_{50}$ electrocatalyst has also demonstrated catalytic activity as cathode in a single PEMFC. The performance achieved with anodic and cathodic loading of 1.0 mg cm^{-2} was 210 mW cm^{-2} at 0.35 V and 80 °C. This value is about the half of the performance reported with Pt under the same experimental conditions.

Acknowledgements

This work was financially supported by Mexican Council of Science and Technology, CONACYT (Grant No. 101537) and Science and Technology Institute of Mexico City, ICYTDF (Grant OSF). JJSP thanks CONACYT for doctoral fellowship.

References

[1] K. Suárez-Alcántara, O. Solorza-Feria, Electrochim. Acta 53 (2008) 4981.
[2] J. Kim, T. Momma, T. Osaka, J. Power Sources 189 (2009) 909.
[3] K. Suárez-Alcántara, O. Solorza-Feria, J. Power Sources 192 (2009) 165.
[4] A. Sarkar, A.V. Murugan, A. Manthiram, J. Mater. Chem. 19 (2009) 159.
[5] G. Vázquez, O. Solorza-Feria, J. New Mater. Electrochem. Syst. 12 (2009) 17.
[6] V. Collins-Martínez, R.G. González-Huerta, A. López-Ortiz, D. Delgado-Vigil, O. Solorza-Feria, J. New Mater. Electrochem. Syst. 12 (2009) 63.
[7] A. Gebert, N. Mattern, U. Kuehn, J. Eckert, L. Schultz, Intermetallics 15 (2007) 1183.
[8] X. Wang, N. Kariuki, J.T. Vaughev, J. Goodpaster, R. Kumar, D.J. Myers, J. Electrochem. Soc. 155 (2008) B602.
[9] A. Sarkar, A. Murugan, A. Manthiram, J. Mater. Chem. 19 (2009) 159.
[10] F.P. Hu, Z. Wang, Y. Li, Ch. Li, X. Zang, P.K. Shen, J. Power Sources 177 (2008) 61.
[11] J.J. Salvador-Pascual, S. Citalán-Cigarroa, O. Solorza-Feria, J. Power Sources 172 (2007) 229.
[12] G. Ramos-Sánchez, H. Yee-Madeira, O. Solorza-Feria, Int. J. Hydrogen Energy 33 (2008) 3596.
[13] J.J. Salvador-Pascual, A. Chávez-Carvayar, O. Solorza-Feria, ECS Trans. 15 (2008) 3.
[14] L. Jiang, Z. Zhou, W. Li, W. Zhou, S. Song, H. Li, G. Sun, Q. Xin, Energy Fuels 18 (2004) 866.
[15] A.C. Bernardes-Silva, A.F. De Mesquita, E. Moura, A.O. Porto, G.M. De Lima, J.D. Ardisson, F.S. Lameiras, Solid State Commun. 135 (2005) 687.
[16] R.G. González-Huerta, R. González-Cruz, S. Citalán-Cigarroa, C. Montero-Ocampo, J. Chávez-Carvayar, O. Solorza-Feria, J. New Mater. Electrochem. Syst. 8 (2005) 15.
[17] R.G. González-Huerta, J.A. Chávez-Carvayar, O. Solorza-Feria, J. Power Sources 153 (2006) 11.
[18] U.A. Paulus, T.J. Schmidt, H.A. Gasteiger, R.J. Behm, J. Electroanal. Chem. 495 (2001) 134.
[19] S.K. Zecevic, J.S. Wainright, M.H. Litt, S.L. Gojkovic, R.F. Savinell, J. Electrochem. Soc. 144 (1997) 2973–2982.
[20] N.M. Marcovic, H.A. Gasteiger, P.N. Ross Jr., J. Phys. Chem. 99 (1995) 3411–3415.
[21] C. Couteanceau, P. Crouigneau, J.-M. Léger, C. Lamy, J. Electroanal. Chem. 379 (1994) 389.